運輸省港湾技術研究所

港湾技術研究所報告

REPORT OF THE PORT AND HARBOUR RESEARCH INSTITUTE

MINISTRY OF TRANSPORT

VOL. 32 NO. 4 DEC. 1993

NAGASE, YOKOSUKA, JAPAN

港湾技術研究所報告 (REPORT OF P.H.R.I)

第32巻　第4号 (Vol.32, No.4), 1993年12月 (Dec.1993)

目　次　(CONTENTS)

REPORT OF PORT AND
HARBOUR RESEARCH INSTITUTE
Vol.32, No.4 (Dec. 1993)

1. Dynamic Soil and Water Pressures due to Saturated Backfills on Non-Yielding Rigid Vertical Walls

Isao ISHIBASHI*
Tatsuo UWABE**
Makoto OSADA***
and Takemitsu TAKANO****

Synopsis

One directional (horizontal) shaking table experiments were conducted on saturated two cohesive and one sandy backfills to investigate the dynamic water and total lateral pressures against rigid non-yielding walls during earthquakes.

It was recognized that the dynamic water pressure is generated due to two different sources. The first source is Westergaard-type, which is due to the flow of free water in non-deformable backfill soil skeleton and the second one is due to the deformability of backfill soil skeleton under nearly undrained condition. For highly permeable backfill soils, the first source dominates in the generation of pore pressure and the second source dominates for cohesive backfills.

The magnitude of the first type is expressed as a function of the parameter, $2\pi n\gamma_w H_w^2/E_w kT$ and the pressure distribution is a reduced shape of the Westergaard solution, where n is the porosity of soil, γ_w is the unit weight of water, H_w is the depth of water table to the impermeable base in the backfill, E_w is the compressibility of water, k is the coefficient of permeability of backfill soil, and T is the period of vibration.

The distribution of the second type is in a bulged form with a peak value at an upper section of the backfill depth. The dynamic water pressure resultants of this type for cohesive backfills are nearly as much as the value of the Westergaard's one but is applied around at 0.6 H from the bottom of soil layer.

The dynamic total pressure resultants for cohesive backfills are nearly twice of the Westergaard's dynamic water pressure resultant and also applied at 0.6 H from the bottom of the soil layer. Dynamic water and total pressures and their points of application of the resultant are not significantly affected by the applied vibrating frequency and the coefficient of volumetric compressibility m_v .

Key Words : Dynamic Earth Pressure, Dynamic Water Pressure, Earthquake, Retaining Structure, Cohesive Soil, Sandy Soil, Saturated Soil, Shaking Table Experiment

*Professor of Department of Civil and Environmental Engineering, Old Dominion University
**Chief of Earthquake Disaster Prevention Laboratory, Structural Engineering Division
***Former Member of Earthquake Disaster Prevention Laboratory, Structural Engineering Division
****Member of Earthquake Disaster Prevention Laboratory, Structural Engineering Division

港湾技術研究所報告
第32巻第4号 (1993. 12)

1．水中の剛な鉛直壁に作用する裏込土の地震時土圧と動水圧

石橋　勲*
上部達生**
長田　信***
高野剛光****

要　旨

水中の剛な壁に作用する裏込め土の動水圧，土圧を検討する事を目的として，2種類のシルト質砂と1種類の砂について振動実験を実施した。結果は以下の通りである。壁体に作用する裏込め土の間隙水による動水圧にはWestergaard式で与えられるもの（土の粒子の骨格の変形に関係しない，水の移動によるもの）と，ほぼ非排水状態での粒子の骨格の変形に起因するものとがあり，透水性の高い土では前者が卓越し，細粒分の多い土では後者が卓越することが確認された。透水性の高い土の間隙水による動水圧は，$2\pi n\gamma_w H_w^2/E_w kT$をパラメータとしたWestergaard式と同様な分布で与えられる。ここにnは空隙率，γ_wは水の単位体積重量，H_wは裏込土層での水深，E_wは水の体積弾性率，kは透水係数，Tは振動周期である。細粒分の多い土の間隙水による動水圧の合力値はWestergaard式のそれとほぼ近いものであるが，その分布は上の部分が大きい形を示し，合力の作用点は裏込め土の高さの0.6倍の位置であった。水中の壁体に地震時に作用する細粒分の多い裏込め土の合力は，Westergaard式で計算される動水圧合力のほぼ2倍の値を示し，この合力の作用点は裏込め土の高さの0.6倍の高さの位置であった。この合力の値，作用点の位置は入力地震動の振動数，あるいは裏込め土の体積圧縮係数の影響をほとんど受けない事が確認された。

キーワード：地震時土圧，動水圧，地震，擁壁，粘性土，砂質土，飽和土，振動実験

*オールドドミニオン大学土木環境工学科教授
**構造部　地震防災研究室長
***前構造部　地震防災研究室（現第一港湾建設局）
****構造部　地震防災研究室

Contents

1. Introduction

A great number of waterfront structures have suffered from damage during past earthquakes in the world. Damages at Akita port during the Nipponkai-Chubu earthquake (M = 7.7) are good examples (Tsuchida et al.[1], 1985). Many quaywalls were tilted and concrete aprons were crushed. Those damages are attributed mostly to the underestimation of the dynamic earth and water pressures against retaining structures in the current aseismic design procedure.

Since Mononobe and Okabe introduced the dynamic lateral earth pressure theory in the mid-1920's, there have been many researches conducted in this area theoretically and experimentally. However, many countries still use basically Mononobe-Okabe's approach as the aseismic design code for retaining structures. Ishibashi and co-researchers[2,3] have summarized the current knowledge on the dynamic lateral earth pressure, they also pointed out the shortcomings of Mononobe-Okabe theory, and proposed the modifications on it.

In the past many researches have been focused studies on dry granular backfill soils. There are very little research results on saturated soils. In particular cases of saturated non-granular (silty to clayey soils) backfills are hardly treated experimentally.

This experimental study examines the theoretical concept proposed earlier by Ishibashi and co-researchers [2,3] on the dynamic water pressure generated in a variety of backfill soil types covering from gravel to clayey soils. The experiments include one-directional horizontal shaking table tests on a rigid non-yielding retaining wall model with sandy and cohesive backfills at Port and Harbour Research Institute, Ministry of Transport, in Japan.

2. Background Studies

The current method in estimating dynamic water pressure and dynamic earth pressure against rigid retaining structures uses two separate concepts; (1) for highly permeable granular backfill soils such as gravels and sands, to use the buoyant unit weight of backfill soil for the dynamic earth pressure calculation, and additionally to apply total Westergaard's dynamic water pressure from the landward side of the retaining structures, and (2) for low permeable cohesive backfill soils such as clayey soils, to use the total unit weight of the backfill for dynamic earth pressure calculation, and not to add any additional dynamic water pressure.

There are no intermediate solutions to cover intermediate soil types such as fine sand and silt in the above approach. In order to overcome this shortcoming, Ishibashi and co-researchers[2,3] have proposed a theory to cover dynamic earth and water pressures for the both regions of soil types. The theory is called "Generalized Apparent Seismic Coefficient Theory" in short.

The theory basically handles the movement of free water in the soil skeleton as the major source of dynamic water pressure generation. In the theory, under dynamic loading, the pore water of saturated soil may be classified into two categories on the basis of its hydrodynamic behavior:(1) free water, which behaves freely with less or no boundary effects due to surrounding soil particles, and of which pressure is induced hydrodynamically by the earthquake excitation, and (2) restricted water, which is strongly influenced by the surface of soil particles and behaves like a part of the soil particles upon application of vibration. For highly permeable soil such as gravel and coarse sand, most of the pore water may belong to the free water category. For less permeable soil such as silt and clay, the majority of the pore water may be classified as restricted water in the above definitions.

A parameter m, is introduced as the volumetric ratio of restricted water to the whole of the void, and takes values between 0.0 to 1.0(m=0.0 for highly permeable soils and m=1.0 for very low permeable soils). The value of m may be affected by factors controlling the hydrodynamic behavior of the pore water, such as grain

size, permeability, rate of loading, etc. Accordingly, it is assumed that: (1) the dynamic water pressure against the wall induced during an earthquake is proportional to the volume of the free water, i.e., (1−m), (2) the hydrodynamic behavior of the free water induced by the earthquake is conformed by Anzo's theory[4], and (3) Anzo's theory is approximated by a simple equation:

$$\frac{P_{wd}}{k_h\gamma_w H_w^2}=0.25-0.265\tanh\left(\log\frac{2\pi n\gamma_w H_w^2}{7E_w kT}\right) \tag{1}$$

where n is the porosity of soil, γ_w is the unit weight of water, H_w is the depth of water table to the impermeable base in the backfill, E_w is the compressibility of water, k is the coefficient of permeability of backfill soil, and T is the period of vibration. From the above assumptions. By knowing the range of m ($0 \leq m \leq 1$), the constant A is 0.5 and the value of m then becomes:

$$m=0.5+0.53\tanh\left(\log\frac{2\pi n\gamma_w H_w^2}{7E_w kT}\right) \tag{2}$$

It should be noted that Anzo's hydrodynamics solution includes three basic assumptions; (1) dynamic pore water pressure during the vibration will be induced only by the flow of the pore water between soil particles, (2) the backfill soil will not deform during the vibration, and (3) Darcy' law is valid for the flow of the pore water.

The following slightly modified version of Anzo's equation is recommended for use:

$$\frac{P_{wd}}{k_h\gamma_w H_w^2}=0.543(1-m)=0.272-0.288\tanh\left(\log\frac{2\pi n\gamma_w H_w^2}{7E_w kT}\right) \tag{3}$$

The modification in the above equation was made so that the $P_{wd}/k_h\gamma_w H_w^2$ value becomes equal to Westergaard's exact value, 0.543 at $m=0$. The above equation is referred as $(1-m)$xWestergaard later in this paper.

The readers may refer to the previous publications (Ishibashi et al.[3] and Matsuzawa et al.[2]) for the detailed development and discussion of the theory.

3. Experimental Procedures

3.1 Shaking Table

The shaking table with 4 m x 3.5 m loading platform used for this study is of an electromagnetic type at the Port and Harbour Research Institute (PHRI), Japan. **Photo.1** shows the shaking table. The table is capable to shake a maximum load of 40 tonf with a maximum acceleration of 0.45 times of the gravitational acceleration in one horizontal direction with a frequency range of 1 to 100 Hz.

3.2 Backfill Soil Types

Six series of shaking table tests were conducted during this study; Niigata, MS2-1, MS2-2, KY3-1, KY3-2, KY3-3. Five of them (MS and KY Series) were for the dynamic water and total pressure measurements due to non-granular backfills, the other (Niigata Test) was for that due to a granular backfill. Two types of soil were used as the non-granular backfills. One was taken from Narita city and called as Musashino (MS) soil, the other from Yokohama city and called as Koyasu (KY) soil. For Koyasu soil, some amounts of the fines were washed out after each series of the experiments so that the permeability of the model backfill was changed; that is, KY3-1 has more fines than KY3-2, and KY3-2 has more fines than KY3-3. Niigata sand was used for the model test of the granular backfill. The grain size distribution curves of each soil are shown in **Fig.1**.

Table.1 summaries properties of the above series of the experiments, where 3D-FEM data is included. 3D-FEM is three dimensional finite element model calculations to simulate those shaking table experiments.

Consolidation test information are from settlement curves during the specimen preparation period in the soil bin. The permeability tests were carried out for specimens in the soil bin after each of the shaking table experiments.

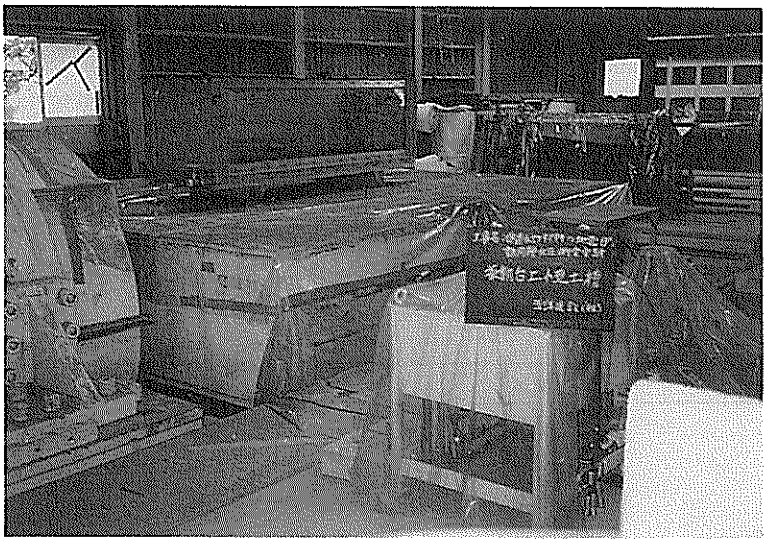

Photo.1 Shaking Table and Soil Bin

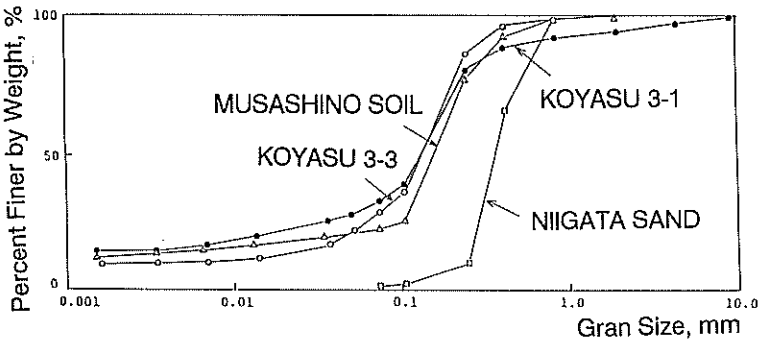

Fig.1 Grain Size Distribution Curves for Soils Tested

Table.1 Soil Properties Tested on Shaking Table

Soil Type	Test I.D.	G_s	w(%)	γ(sat) (gf/cm³)	e	soil Thickness H_s(cm)	δ(cosol) H_s (%)	Permeability k(cm/sec), average		m_v (cm²/gf)	Resonant Frequency (Hz)	Shear Modulus* G (gf/cm²)	c_v (cm²/sec)
								Consl. Data	In-situ				
Musashino	2-1	2.713	44.4	1.777	1.205	40.54	10.9	2.70×10^{-6}	2.90×10^{-6}	1.64×10^{-3}	27	34,700	0.00164
	2-2	2.713	44.6	1.775	1.210	40.73	11.0	2.36×10^{-6}	3.20×10^{-6}	1.64×10^{-3}	24	27,700	0.00142
Koyasu	3-1	2.686	33.5	1.887	0.900	43.76	5.2	1.04×10^{-6}	2.15×10^{-6}	0.831×10^{-3}	12	8,487	0.00127
	3-2	2.686	30.5	1.927	0.819	42.70	5.7	2.37×10^{-6}	3.85×10^{-6}	0.908×10^{-3}	3	512	0.00261
	3-3	2.686	31.6	1.912	0.849	38.47	1.1	1.20×10^{-5}	1.80×10^{-5}	0.184×10^{-3}	28	36,200	0.00354
Niigata		2.773	6.6	1.957	0.852	81.3					21	87,950	
3D-FEM				1.850		40.0					28	10,000	

* $G=\rho(4Hf)^2$

3.3 Model Preparation and Instrumentation

(1) Tests for Musashino and Koyasu Soils

Fig.2 shows locations of instruments for Musashino and Koyasu soil tests. In these tests, a soil bin(2.0 m long, 0.6 m wide, and 0.6 m high) was rigidly fixed on the top of the shaking table platform as shown in **Photo. 1**. Distributions of dynamic pore water pressure and earth pressure were measured by water pressure transducers (diaphragm diameter = 6 mm) and earth pressure transducers (diaphragm diameter = 25 mm) that were placed on the surface of an acrylic board. The whole acrylic board was fixed on a load cell to measure the total thrust on it. **Photo.2** shows the acrylic board and transducers. It shall be noted that the soil pressure transducer measures total (soil as well as water) pressure so that this pressure is hereafter referred as the total pressure.

After placing the instruments, the thoroughly pre-mixed soils were poured into the bin. These soils were too soft for the model tests at that stage so that the model backfill was consolidated before the shaking table tests. On the bottom of the bin, a 7 cm thick gravel layer was packed with No. 7 crushed stone for drainage. The

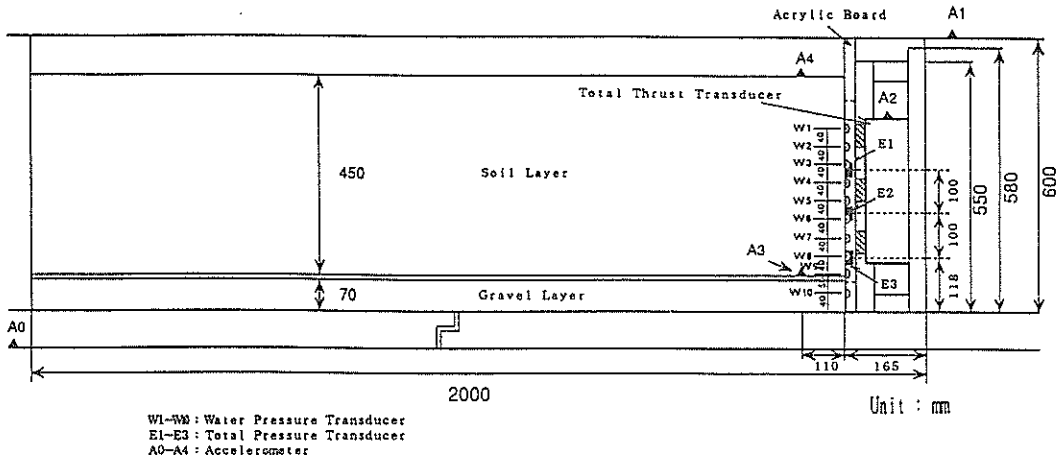

Fig.2 Instrumentation for Musashino and Koyasu Soil Tests

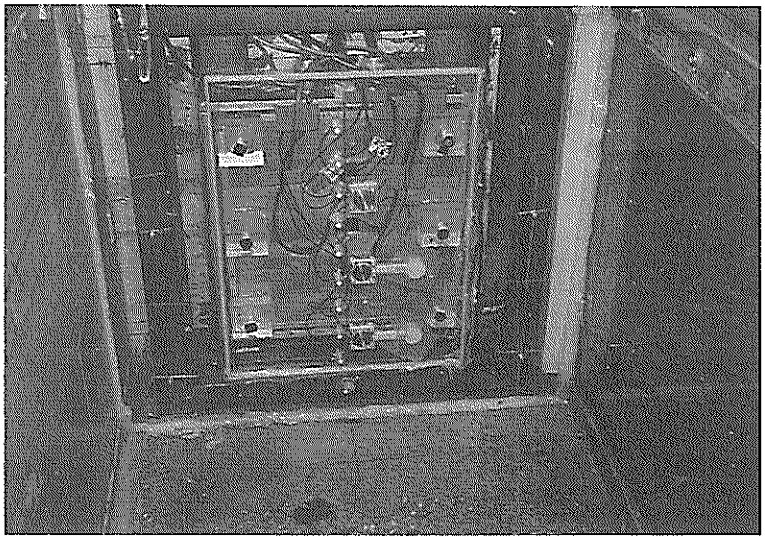

Photo.2 Instrumentation

model backfill was consolidated with 60 gf/cm² (5.9 kPa) surcharge load by using a plastic water bag as shown in **Photo.3**. Settlement of the backfill was measured by displacement transducers to calculate the coefficient of volumetric compressibility of the model ground. Input motions used for the shaking table tests were 10 cycles of sinusoidal wave form with 1, 3, 5, 10, 15, and 20 Hz. The maximum accelerations of the input motion were 50 and 100 gals.

In order to measure the accurate permeability of the model ground, permeability tests were conducted after the shaking table tests. A thin wall metal tube was pushed into the model ground slowly and carefully to the top of the gravel layer. The section above the model ground surface of the thin wall tube was filled with water. The water level change and elapsed time were monitored (falling head permeability test) and the coefficients of permeability were then calculated.

(2) Test for Niigata Sand

A large soil bin (3.0 m long, 1.5 m wide, and 1.2 m high) was used for Niigata sand test. **Fig.3** shows the locations of instruments. A 80 cm thick model ground was constructed on the top of 20 cm thick gravel layer. Water pressure transducers and earth pressure transducers were placed on a rigid board, which was fixed on the side of the soil bin. Input motions used for this series were 10 cycles of sinusoidal wave form with 2, 3, 6, 10, 20, and 40 Hz. The maximum acceleration of the input motion was 20 gals.

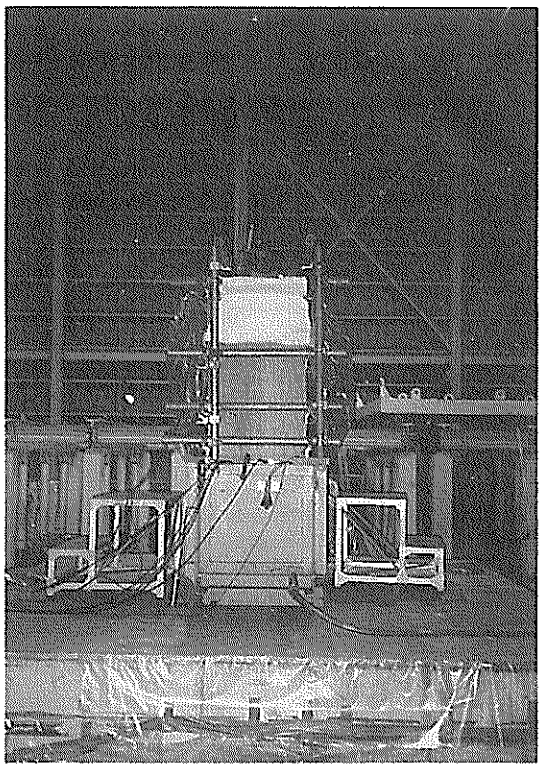

Photo.3 Consolidation

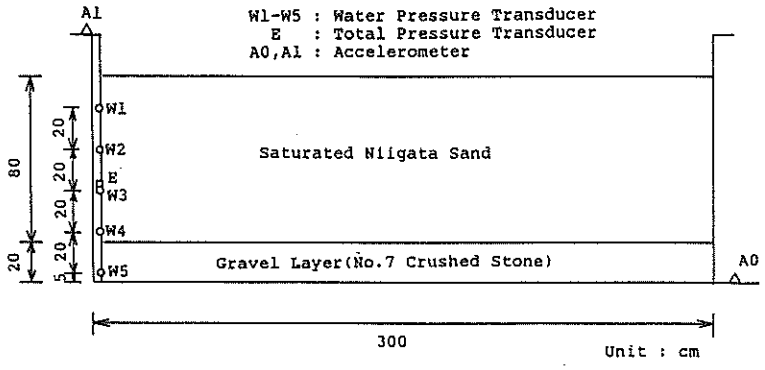

Fig.3 Instrumentation for Niigata Sand Test

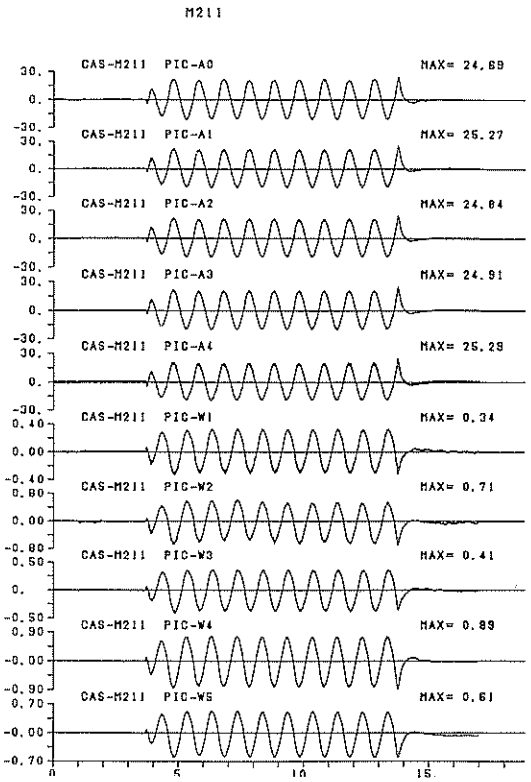

Fig.4(a) Measured Raw Data on Shaking Table Experiment

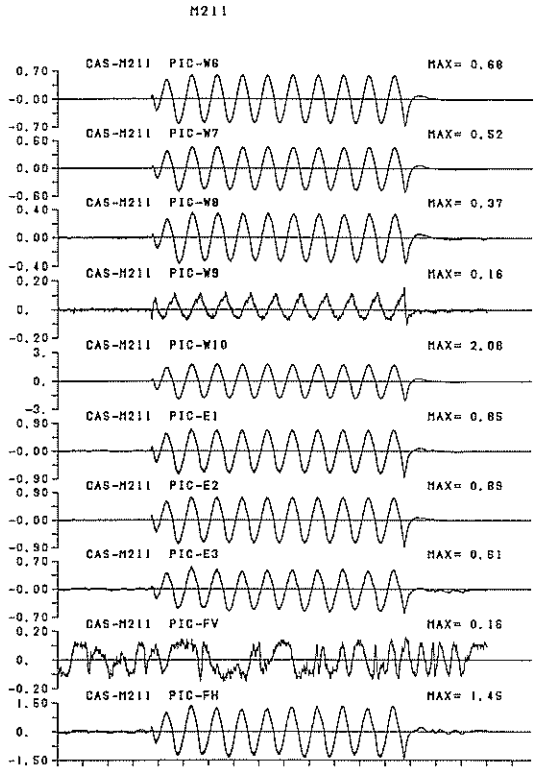

Fig.4(b) Measured Raw Data on Shaking Table Experiment

4. Data Reduction and Test Results

4.1 Measured Raw Data Reductions

Figs.4 (a) and **(b)** show typical measured raw data with time during a shaking table experiment. It includes five accelerations (A0, A1, A2, A3, A4), nine pore water pressures (w1 through w9) in the soil layer, one pore water pressure (w10) in the gravel layer, three total pressures (E1, E2, E3), and two total thrusts (*Fh* and *Fv*) on the pressure board. The vertical component of the total thrust *Fv* was negligibly small (less than 10 % of

Fh) so that it was not used in the further analyses. The measured horizontal component of the total force Fh was corrected by its horizontal acceleration inertia effect, which was obtained by measuring its inertia force without any backfill during horizontal shaking. For the pore water pressure and total pressure transducers it was found that inertia corrections were not needed, so that no corrections have been applied.

In order to avoid the effect of significant permanent pore water pressure buildup due to soil liquefaction phenomenon particularly for granular materials, the first peak records were used for the further analyses. All the data were taken at the exact time when the acceleration record at the top of gravel layer A3 reached its first peak. Therefore, it is not necessary that all the data reach their peak values at the exact same time. In general, most of the records did not show any meaningful time lag except the one for w9.

4.2 Dynamic Water Pressure

Dynamic water pressure is defined as the vibrating amplitude of pore water pressure measurements and thus it excludes initial static water pressure. **Fig.5(a)** shows measured dynamic water pressure divided by its peak horizontal acceleration coefficient k_h with depth for various vibrating frequencies tested for Musashino 2-1 test, where k_h is the ratio of the horizontal acceleration to the gravitational acceleration. Westergaard's exact solution is also plotted for comparison purposes.

In the design of port structures in Japan the following approximate solutions proposed by Westergaard are used for the dynamic water pressure distribution, p_{wd} and the resultant dynamic water pressure, P_{wd}:

$$p_{wd}=\frac{7}{8}k_h\gamma_w\sqrt{H_w x} \tag{4}$$

$$P_{wd}=\frac{7}{12}k_h\gamma_w H_w^2 \tag{5}$$

in which γ_w is the unit weight of water; x is the depth of water; H_w is the total depth of water.

4.3 Dynamic Total Pressure

Fig.5(b) shows measured dynamic total pressure (divided by k_h) distribution for Musashino 2-1 test. In the figure zero value at the top of the soil layer and the next datum is connected. Since the total horizontal thrust F_h is measured, integrated pressure along the depth shall be equal to F_h. Accordingly the following modifications on p/k_h - z curves are made. For the lower portion in the curves, the curves are linearly extended to the

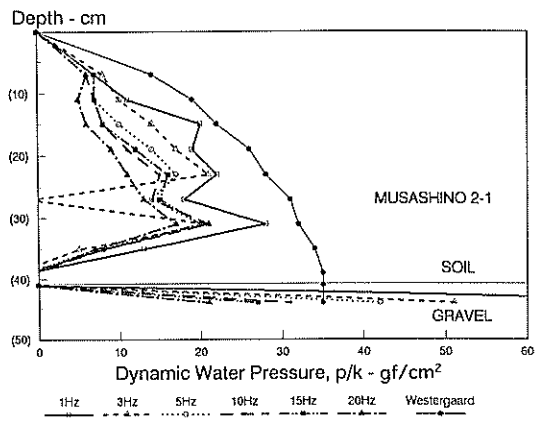

Fig.5(a) Dynamic Water Pressure Distributions for Musashino 2-1

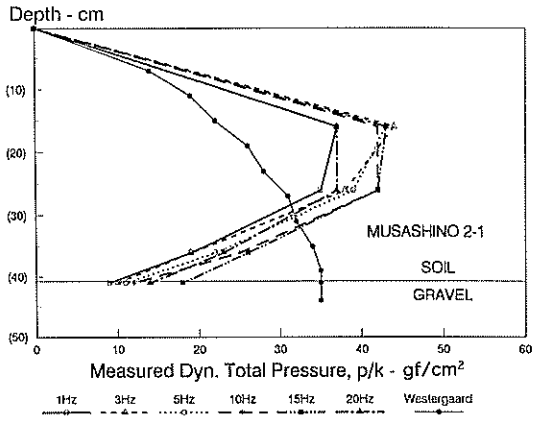

Fig.5(b) Dynamic Total Pressure Distributions for Musashino 2-1

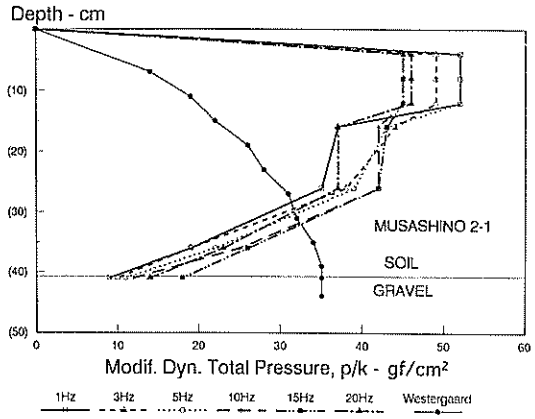

Fig.5(c) Modified Dynamic Total Pressure Distributions for Musashino 2-1

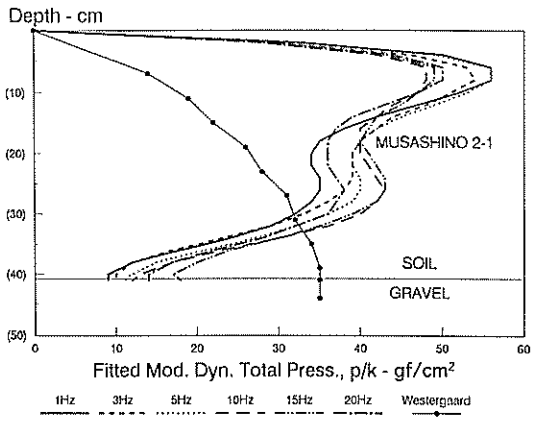

Fig.5(d) Fitted Curves of Modified Dynamic Total Pressure Distribution for Musashino 2-1

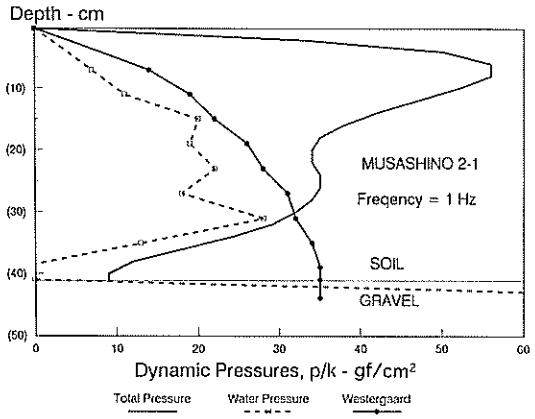

Fig.5(e) Dynamic Total and Water Pressure Distributions with f=1 Hz for Musashino 2-1

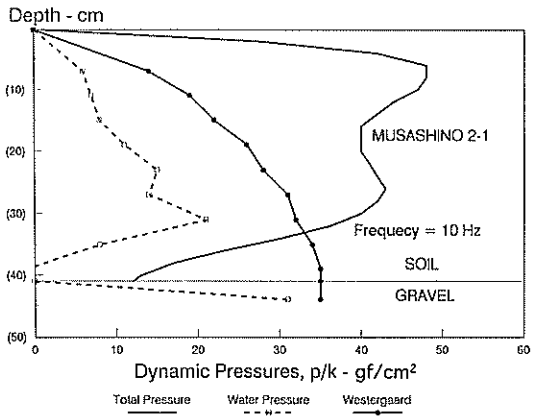

Fig.5(f) Dynamic Total and Water Pressure Distributions with f=10 Hz for Musashino 2-1

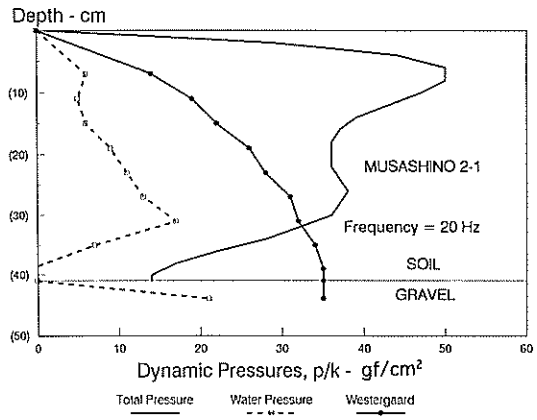

Fig.5(g) Dynamic Total and Water Pressure Distributions with f=20 Hz for Musashino 2-1

bottom of the soil layer. For the upper portion, at four equally spaced sections above El data point, equal total pressures are distributed so that the integrated pressure along the total depth becomes equal to the measured total horizontal thrust F_h. **Fig.5(c)** shows such plots. Since the upper section of the curves shall be smooth one, the data points are further smoothed out by fitting with 5th degree polynomials. **Fig.5(d)** shows those fitted curves. In the following discussions, we only show those fitted curves for total pressure distribution. However, we use the total resultant thrusts based on measured F_h values and calculate the point of application of the resultant based on the curves such as **Fig.5(c)**.

4.4 Dynamic Soil Pressure

Dynamic soil pressure is defined as the dynamic total pressure minus dynamic water pressure. It shall be noted that this definition might be a fictitious one and it may not necessarily mean the lateral pressure associated with purely soil's buoyancy inertia component. It may include more complex interaction effect between soil and water phases.

4.5 Presentation of Test Results

Fig.5(e), **(f)** and **(g)** are redraws of total and water pressure distributions for Musashino 2-1 test with vibrating frequencies of 1, 10, and 20 Hz, respectively. In those figures the difference between the total pressure curve and the water pressure curve is called as the dynamic soil pressure as defined in 4.4

In the followings, similar sets of figures as for Musashino 2-1 test are presented for different test series; **Fig.6** for Musashino 2-2 test, **Fig.7** for Koyasu 3-1 test, **Fig.8** for Koyasu 3-2 test, **Fig.9** for Koyasu 3-3 test, and **Fig.10** for Niigata Sand test. Each of the above figures except Niigata Sand test includes (a) dynamic water pressure distributions with various frequencies, and (b) dynamic total pressure distributions (fitted curves) with various frequencies. For Niigata Sand test, since only one total pressure is measured in **Fig.10(b)**, dynamic total pressure distributions were not generated.

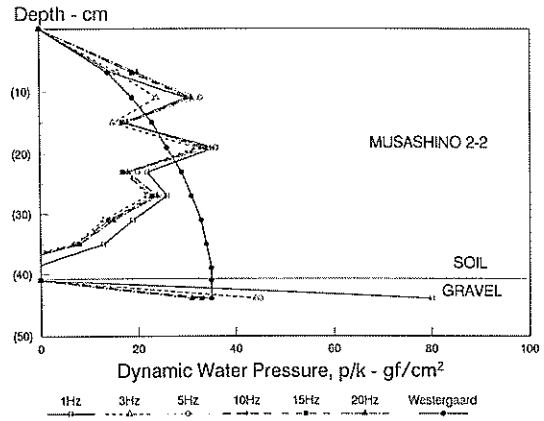

Fig.6(a) Dynamic Water Pressure Distributions for Musashino 2-2

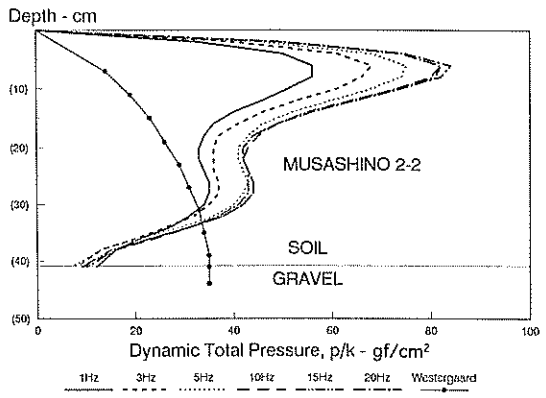

Fig.6(b) Dynamic Total Pressure Distributions for Musashino 2-2

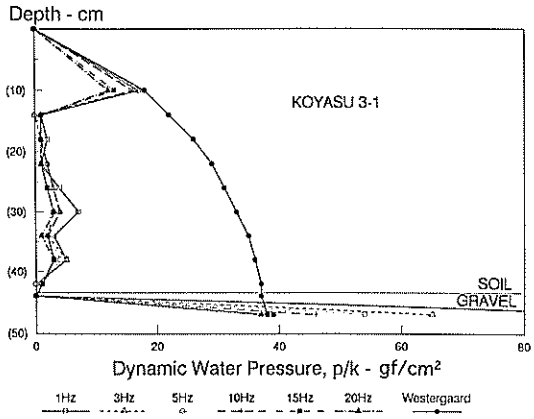

Fig.7(a) Dynamic Water Pressure Distributions for Koyasu 3-1

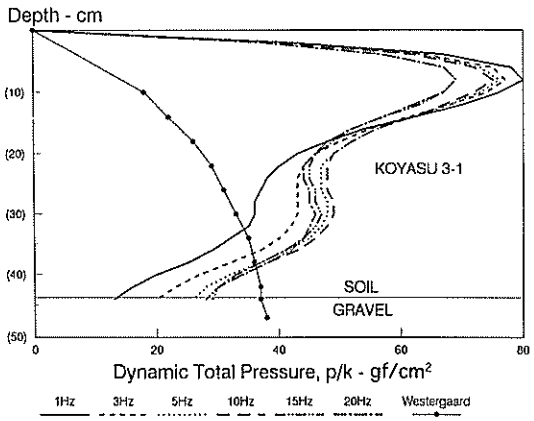

Fig.7(b) Dynamic Total Pressure Distributions for Koyasu 3-1

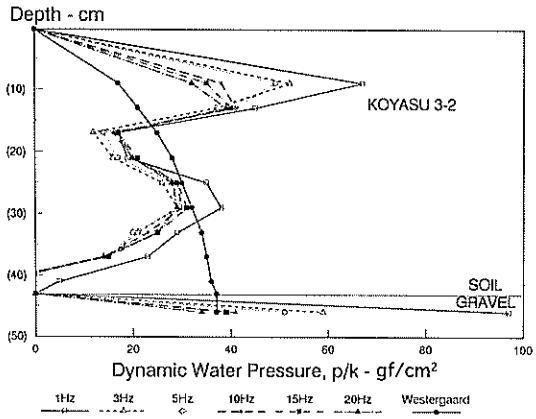

Fig.8(a) Dynamic Water Pressure Distributions for Koyasu 3-2

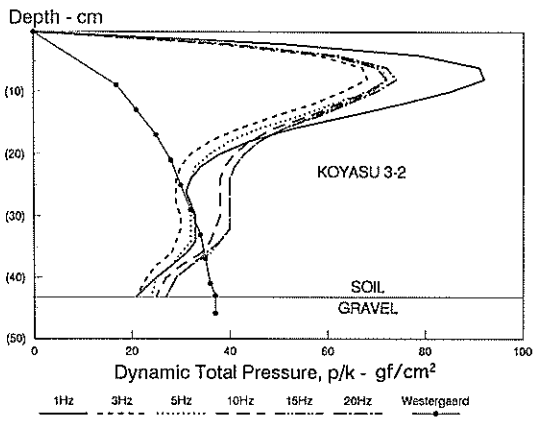

Fig.8(b) Dynamic Total Pressure Distributions for Koyasu 3-2

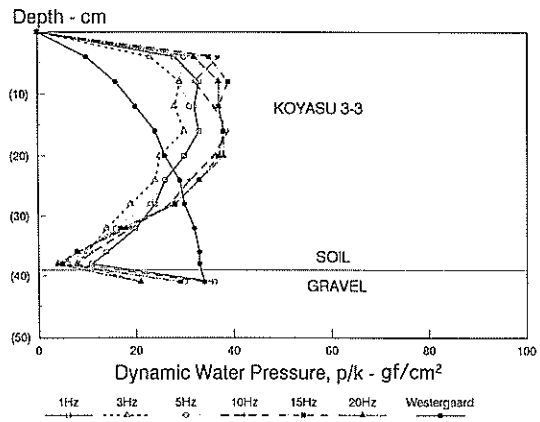

Fig.9(a) Dynamic Water Pressure Distributions for Koyasu 3-3

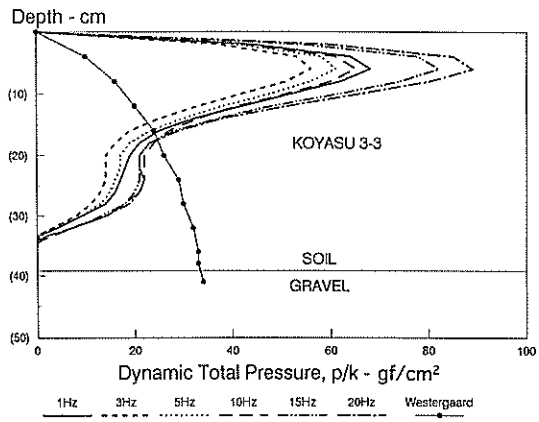

Fig.9(b) Dynamic Total Pressure Distributions for Koyasu 3-3

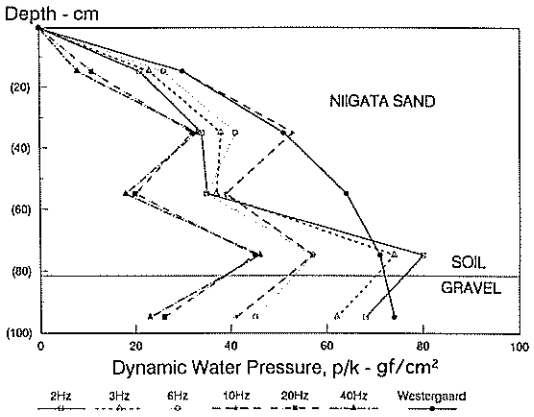

Fig.10(a) Dynamic Water Pressure Distributions for Niigata Sand

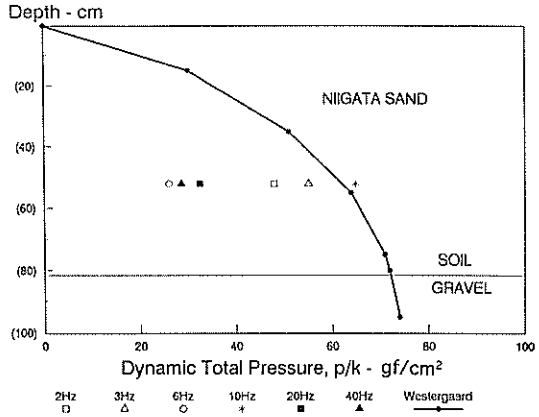

Fig.10(b) Dynamic Total Pressure Distributions for Niigata Sand

5. Discussions

5.1 Dynamic Water Pressure due to Non-Deformable Backfills

Ishibashi and other's concept for dynamic water pressure as described previously implies that the dynamic water pressure will decrease with increasing a non-dimensional parameter $2\pi n\gamma_w H_w^2/E_w kT$ and it is expressed as a certain reduction from the Westergaard's value as seen in Eq.3. If others are the same, the dynamic water pressure shall decrease when the permeability of the backfill becomes low. The cohesive backfills of the shaking table model tests have much lower permeability than the one of sandy backfill soils. Dynamic water pressure distribution plots for Musashino and Koyasu soils showed somewhat irregular patterns. In general, those do not follow the distribution shape of the Westergaard's theory. In upper portions along the wall those curves often exceed the Westergaard's curve. Those observation obviously contradicts Ishibashi and others' previous concept.

We shall reexamine the assumptions made on the theory. There are three basic assumptions in the theory; (1) dynamic pore water pressure during the vibration will be induced only by the flow of the pore water between soil particles, (2) the backfill soil will not deform during the vibration, and (3) Darcy's law is valid for the flow of the pore water. It is suspected that the combination of above (1) and (2) assumptions may not be applicable to soft clayey soils. There might be other sources of dynamic water pressure generation in more deformable backfill materials.

When fully saturated backfill material is very deformable, it will generate dynamic water pressure under undrained conditions. The pore water pressure generation under three dimensional stress changes can be calculated by the following equation under totally undrained condition;

$$\Delta u=\frac{1}{n\frac{k_w}{k_s}+1}\frac{\Delta\sigma_1+\Delta\sigma_2+\Delta\sigma_3}{3} \tag{6}$$

where k_w and k_s are coefficients of compressibility of pore water and soil skeleton, respectively. In general, k_w is much smaller than k_s so that Eq. 6 becomes;

$$\Delta u=\frac{\Delta\sigma_1+\Delta\sigma_2+\Delta\sigma_3}{3} \tag{7}$$

For a demonstration purpose, dynamic elastic analyses (3D-FEM) using a three dimensional finite element code in simulating the shaking table experiment were conducted. Dynamic shear modulus for the soil layer was

100 t/m² and that for the gravel layer was 2000 t/m². **Figs.11(a)** and **(b)** show the results for frequency f=3 Hz and f=20 Hz, respectively. Dynamic water pressures were calculated based on Eq. 7 and the total pressures were calculated as the steady state vibrating amplitude of the horizontal normal stress at the central elements along the wall boundary during horizontal sinusoidal vibrations. Similar pressure distribution patterns can be observed as the ones from the shaking table experiments. There are much higher pressures at the upper section of the soil layer and those curves often exceed the Westergaard's solution.

It is theorized that the dynamic water pressure on the vertical rigid wall will be generated by two different sources; (1) due to the flow of pore water through the backfill soil skeleton, and (2) due to deformation of backfill soil skeleton under semi-undrained condition during vibrations. The source (1) will follow the Ishibashi and others' original concept so that the dynamic water pressure distribution shape will follow the Westergaard's theory and the magnitude will be a certain percentage of Westergaard's value depending on the parameter $2\pi n\gamma_w H_w^2/E_w kT$. This type of dynamic water pressure will be a dominant source of dynamic water pressure for coarse granular materials and is called as "Westergaard-type dynamic water pressure" hereafter in this report.

The source (2) dynamic water pressure will distribute in a bulged form with a peak value at an upper section of the depth. Very deformable backfill soil type will contribute much to this category of the dynamic water pressure generation. Soil types tested during this research except Niigata Sand seem to belong to this category.

Koyasu 3-3 and Niigata Sand test data have non-zero dynamic water pressures at the bottom of the soil layers (see **Figs.9(a)** and **10(a)**, respectively), while all others have zero or near zero values at the bottom of the layer. Those non-zero values are considered as the dynamic water pressure generations contributed by the Westergaard-type source as described above. The Westergaard-type dynamic water pressure resultant was calculated from a Westergaard-type distribution form with the maximum value as its non-zero value at the bottom of the soil layer. **Fig.12** plots those two data with various frequencies with the parameter $2\pi n\gamma_w H_w^2/E_w kT$. The data agrees very well with the theoretical $(1-m)$ x Westergaard curve. The m equation is shown in the figure. Most of the pore water pressure generation in Niigata Sand seems to be contributed from this source. The remainder portion in Koyasu 3-3 and nearly all portions in other soil types seem to come from the source (2) in the above discussion.

5.2 Effect of Frequency on Resultants of Dynamic Pressure

Figs.13 through **16** show variations of resultant forces of each dynamic pressure (water pressure, modified water pressure, total pressure, and soil pressure, respectively) over different vibrating frequencies. In the

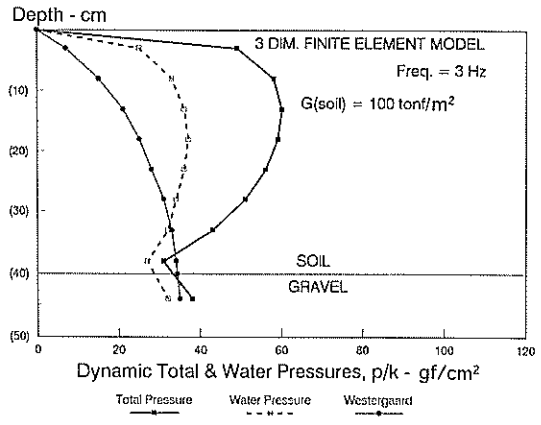

Fig.11(a) Dynamic Total and Water Pressure with f=3 Hz from 3D-FEM Analysis

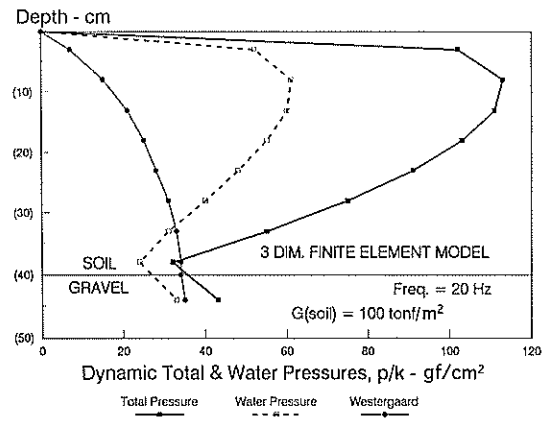

Fig.11(b) Dynamic Total and Water Pressure with f=20 Hz from 3D-FEM Analysis

figures, the actual resultant forces were divided by $\gamma_{saturated} \times H^2$ to obtain non-dimensional values, where $\gamma_{saturated}$ is the unit weight of saturated soil and H is the total height of soil layer. Modified water pressures are reduced by subtracting Westergaard-type dynamic water pressures from the measured dynamic water pressures for Koyasu 3-3 and Niigata Sand cases. There are little changes on those values over the frequency ranges tested (1 to 20 Hz for most of the tests). On the same figures the results from the 3D-FEM analyses are shown. Although those analytical values increase with increasing frequency, the analyses involve many simplification such as perfectly undrained, simple elastic, constant rigidity, etc. Therefore, it is concluded that the effect of frequency on resultant forces of dynamic water, modified water, total, and soil pressures is not significant.

Similarly in **Figs.17** through **20**, the variations of the points of application of the corresponding resultant forces shown in **Figs.13** through **16**, respectively, are plotted with changes of the frequency. Again there is little

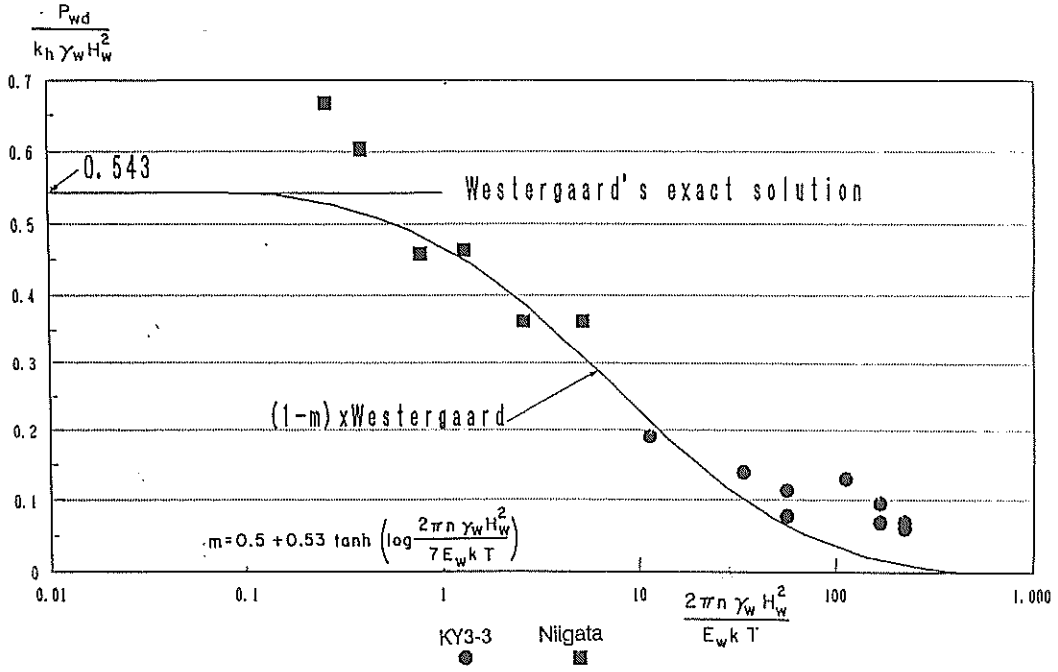

Fig.12 Effect of Permeability on Westergaard-type Dynamic Water Pressure

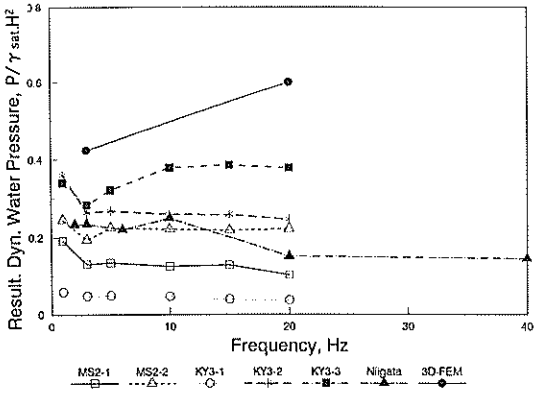

Fig.13 Dynamic Water Pressure Resultant with Frequencies

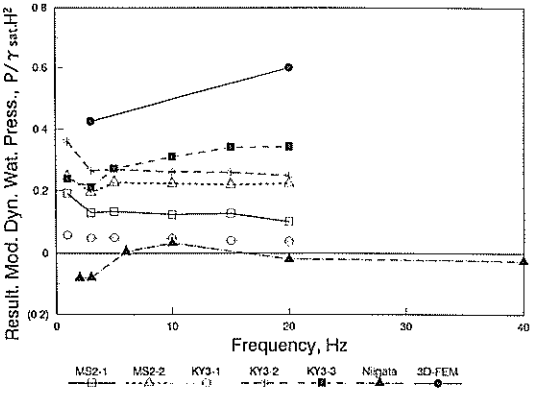

Fig.14 Modified Dynamic WaterPressure Resultant with Frequencies

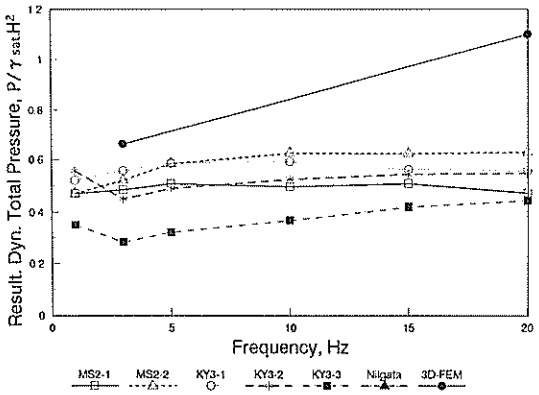

Fig.15 Dynamic Total Pressure Resultant with Frequencies

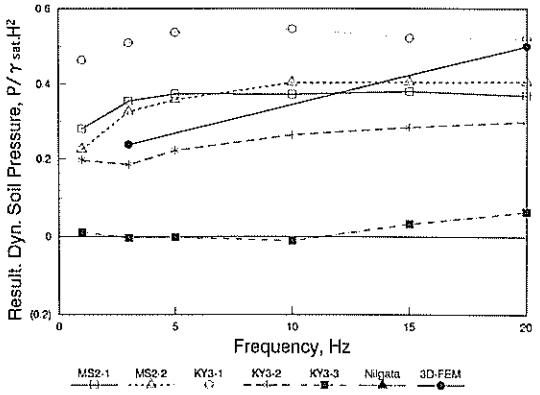

Fig.16 Dynamic Soil Pressure Resultant with Frequencies

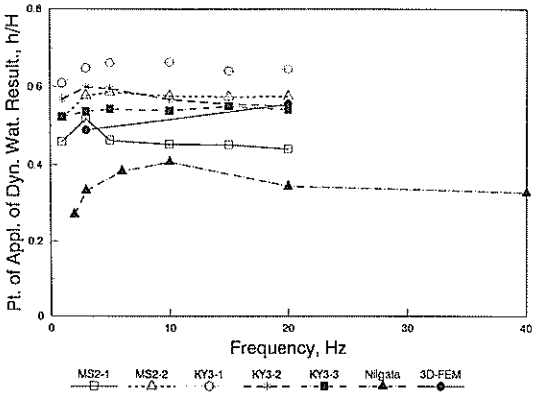

Fig.17 Point of Application of Dynamic Water Pressure Resultant with Frequencies

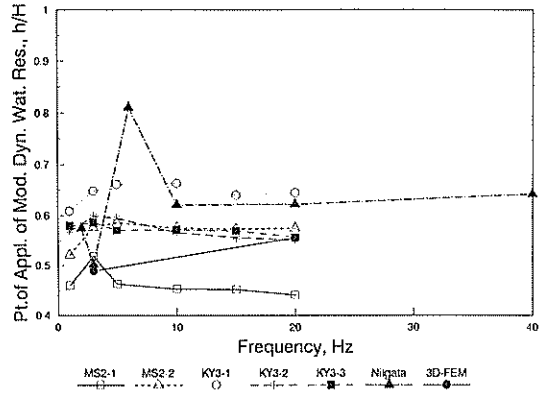

Fig.18 Point of Application of Modified Dynamic Water Pressure Resultant with Frequencies

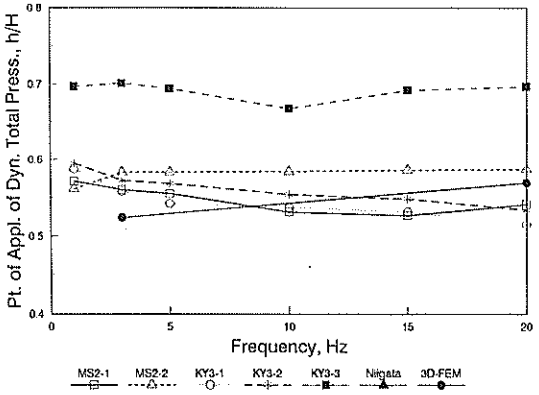

Fig.19 Point of Application of Dynamic Total Pressure Resultant with Frequencies

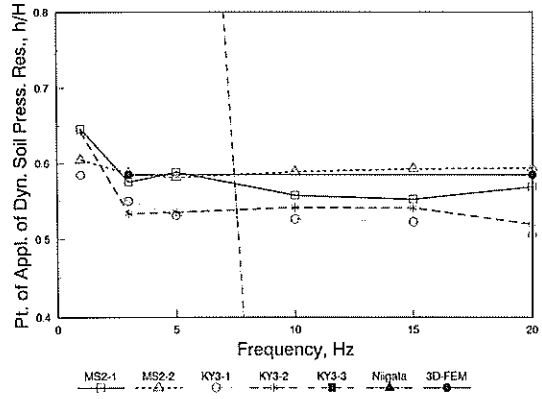

Fig.20 Point of Application of Dynamic Soil Pressure Resultant with Frequencies

frequency effect on those application points of the resultants. In the following discussions, therefore, the averaged values over the applied frequencies are presented.

5.3 Resultant of Dynamic Water Pressure

It is anticipated that the variation on dynamic water pressure might be systematically related to some of soil's parameters. Since the most of the above dynamic water pressures is considered to be stemmed from the deformability of soil skeleton (water pressure generation source (2)), the coefficient of volumetric compressibility m_v is chosen as a possible candidate among many other soil parameters. m_v is defined as the ratio of the porosity change to the effective stress change in one dimensional consolidation theory. **Fig.21** plots relationships between the non-dimensional dynamic water pressure resultant and *log* m_v. **Fig.22** plots a similar one for the modified (subtracted) dynamic water pressure resultant due to the Westergaard-type dynamic water pressure effect. It shall be noted that the Westergaard's solutions in those figures were normalized by the same normalizing parameter $\gamma_{saturated} \times H^2$ as the one for measured resultant forces, where $\gamma_{saturated}$ is the corresponding soil's saturated unit weight but not that of water. Therefore, the non-dimensional Westergaard values differ from its exact coefficient 0.543, which uses γ_{water} for normalization.

In both figures Niigata Sand data were plotted at $m_v = 0.0001$ cm²/gf. Although the m_v value of Niigata Sand is not available, the value will be in a range of 10^{-5} to 10^{-6} cm²/gf. **Fig.21** indicates that, particularly considering the data point of Niigata Sand, dynamic water pressure resultant due to saturated backfills will not be influenced by the coefficient of volumetric compressibility m_v and those values are as much as the Westergaard's resultant. Koyasu 3-1 data is extremely low in comparison with others. It is possible that some experimental errors might be involved; that is, the inside pressurized diaphragm surface of the pore water transducers was not fully saturated since it was the first series of the experiments. **Fig.22** shows that the modified dynamic water pressure by subtracting the Westergaard-type dynamic water pressure will increase from zero for Niigata Sand to about 0.3 for the most of clayey backfills tested during this investigation. The value of 0.3 is nearly the same as the Westergaard's value.

5.4 Resultant of Dynamic Total Pressure

Fig.23 plots non-dimensional resultants of the dynamic total pressure versus *log* m_v. The value slightly increases with increasing m_v. It can be said that the non-dimensional total dynamic pressure resultant, $P/(\gamma_{saturated} \times H^2)$, due to saturated clayey backfill on the vertical non-yielding rigid wall is as high as 0.6, which

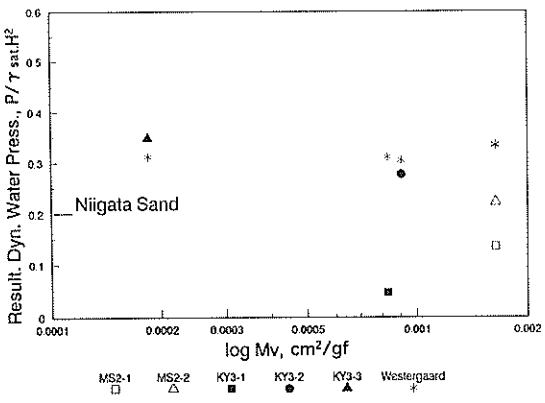

Fig.21 Dynamic Water Pressure Resultant versus m_v

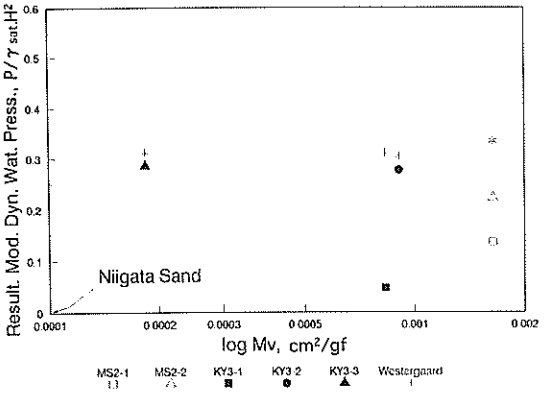

Fig.22 Modified Dynamic Water Pressure Resultant versus m_v

is nearly twice of the Westergaard's dynamic water pressure resultant.

5.5 Point of Application of Resultant Forces

Figs.24, 25, and **26** show the points of application of resultants of dynamic water, modified dynamic water, and dynamic total pressures, respectively, as a function of log m_v. The values are measured from the bottom of the soil layers and normalized by the soil layer thickness H. Nearly all values are 0.6 regardless m_v values except for the dynamic water pressure of Niigata Sand. It shall be noted that the Westergaard's dynamic water pressure resultant is applied at 0.4 H_w from the bottom of the layer.

5.6 Non-Yielding Vertical Wall versus Yielding Vertical Wall

The original intention of the research was to evaluate dynamic water pressure on yielded rigid vertical walls during the horizontal vibration. The vibrating amplitudes of water pressure on yielded (active or passive) wall and on non-yielding wall are considered to be the same unless the relative velocity of the wall to the backfill is large enough to create significant phase differences between the vibration of dynamic water pressure and that of the wall movement (Uwabe et al.[5], 1991). Since the yielded stage is considered as a steady state, the relative

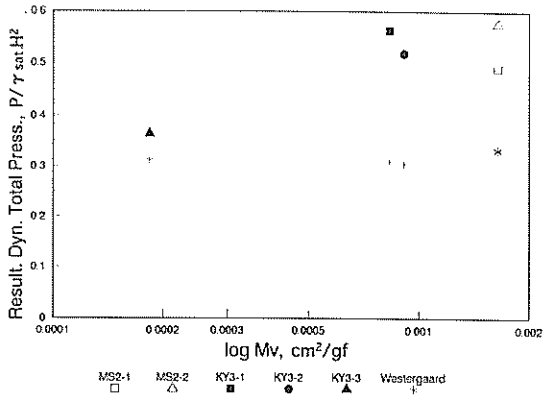

Fig.23 Dynamic Total Pressure Resultant versus m_v

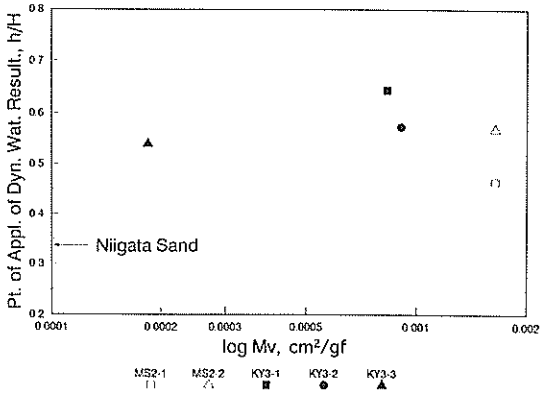

Fig.24 Point of Application of Dynamic Water Pressure Resultant versus m_v

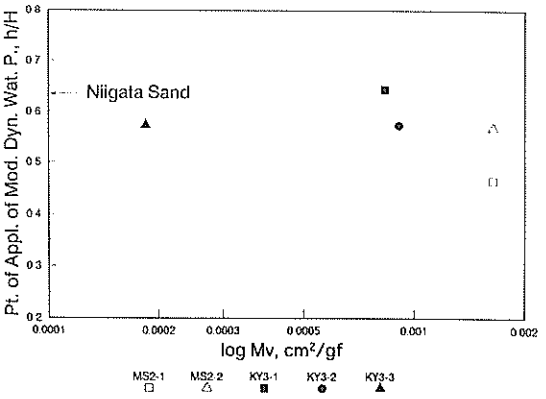

Fig.25 Point of Application of Modified Dynamic Water Pressure Resultant versus m_v

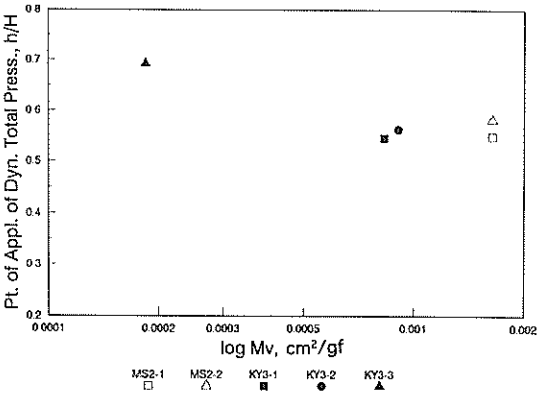

Fig.26 Point of Application of Dynamic Total Pressure Resultant versus m_v

velocity of the wall to the ground shall be small. Therefore, as far as the dynamic water pressure is concerned, the discussions throughout this paper may be applicable to either yielded wall or non-yielded wall. On the other hand, when the total lateral pressure, including dynamic water and dynamic soil pressures, are considered, the discussions in this paper is only the one for non-yielding walls since yielded soil behaves differently from the non-yielded soil.

Dynamic total pressure investigation on yielded rigid walls from saturated cohesive backfills needs additional experimental research. At present these experiments have not been carried out in any place.

6. Conclusions

One directional (horizontal) shaking table experiments were conducted on saturated two cohesive and one sandy backfills to investigate the dynamic water and the total lateral pressures against rigid non-yielding walls during earthquakes. The following conclusions may be drawn from this experimental research;

1. It was recognized that the dynamic water pressure will be generated due to two different mechanisms.
2. The first source is Westergaard-type, which is due to the flow of free water in non-deformable backfill soil skeleton. The major source of the dynamic water pressures will be this type for highly permeable backfill soils such as gravels and sands. The magnitude of this type will be expressed as a function of the parameter, $2\pi n\gamma_w H_w^2/E_w kT$ and the pressure distribution will be a reduced shape of the Westergaard solution.
3. The second dynamic water pressure generation mechanism is due to the deformability of backfill soil skeleton under nearly undrained condition. This mechanism dominates in cohesive backfills. The distribution is in a bulged form with a peak value at an upper section of the depth. The dynamic water pressure resultants of this type for cohesive backfills are nearly as much as the value of the Westergaard's one but is applied around at $0.6\ H$ from the bottom of soil layer.
4. The dynamic total pressure resultants for cohesive backfills are nearly twice of the Westergaard's dynamic water pressure resultant and also applied at $0.6\ H$ from the bottom of the soil layer.
5. Dynamic water and total pressures and their points of application of the resultant are not significantly affected by the applied vibrating frequency and the coefficient of volumetric compressibility m_v.

Acknowledgement

This research was conducted as the U.S.-Japan cooperative research on Seismic Stability of Waterfront Retaining Structures at the Port and Harbour Research Institute (PHRI), Ministry of Transport, Yokosuka, Japan during January through December, 1992. Dr. Isao Ishibashi of Old Dominion University, and Dr. Setsuo Noda and Dr. Tatsuo Uwabe of PHRI are co-principal investigators of the cooperative research. Dr. Ishibashi's visit to PHRI was financially supported by U.S. National Science Foundation and Old Dominion University. The experimental work was financially sponsored by Japanese Science and Technology Agency.

Dr. Kouki Zen of the Soil Dynamics Laboratory at PHRI kindly allowed us to place soil and water pressure transducers on their shaking table experimental setup for Niigata sand.

The Experiments were also assisted by Dr. Masaaki Mito and Mr. Takeshi Sasaki of Penta-Ocean Construction Co., Ltd. and Mr. Kyoji Watanabe of Alpha Engineering Co.

The authors greatly acknowledge the above all supports provided for this joint research project.

References

1) Tsuchida, H., Noda, S., Inatomi, T., Uwabe, T., Iai, S., Ohneda, H., and Toyama, S., "Damage to Port Structures by the 1983 Nipponkai-Chubu Earthquake," Technical Note of the Port and Harbour Research Institute, No.511, March 1985.
2) Matsuzawa, H., Ishibashi, I., and Kawamura, M., "Dynamic Soil and Water Pressure of Submerged Soils," Journal of Geotechnical Engineering, ASCE, Vol. 111, No.10, 1985, pp.1161~1176.
3) Ishibashi, I., Matsuzawa, H., and Kawamura, M., "Generalized Apparent Seismic Coefficient for Dynamic Lateral Earth Pressure Determination," Proceedings of the 2nd International Conference on Soil Dynamics and Earthquake Engineering, edited by C. A. Brebbia, A. S. Cakmak, and A. M. Abdel Ghaffer, QE II, June/July 1985, pp.6-33 ~ 6-42.
4) Uwabe, T., Osada, M., and Takano, T., "Sliding Behavior of Underwater Gravity-type Retaining Structures during Earthquakes," Proceedings of the 26th Annual Meeting of Japanese Society of Soil Mechanics and Foundation Engineering, Nagano, 1991, pp.939~940 (in Japanese).
5) Anzo, Z., " Dynamic Water Pressure against Retaining Walls during Earthquake (In Japanese) ", Proceedings of the third Annual Meeting of Japan Society of Civil Engineers, 1936.

List of Symbols

c_v : the coefficient of consolidation
E_w : the compressibility of water
F_h : the horizontal component of the total force
F_v : the vertical component of the total force
G : the shear modulus
G_s : the specific gravity
H : the total height of soil layer.
H_w : the depth of water table to the impermeable base in the backfill
k : the coefficient of permeability of backfill soil
k_h : the peak horizontal acceleration coefficient
k_s : the coefficient of compressibility of soil skeleton
k_w : the coefficient of compressibility of pore water
m_v : the coefficient of volumetric compressibility
n : the porosity of soil
P : the total dynamic pressure resultant
p : the dynamic water pressure distribution
T : the period of vibration
w : the water content
x : the depth of water
$\gamma_{saturated}$: the unit weight of saturated soil
γ_w : the unit weight of water